Subdomain Model for Predicting Armature Reaction Field of Dual-Stator Consequent-Pole PM Machines Accounting for Tooth-Tips

Minchen Zhu, Lijian Wu, Youtong Fang, and Thierry Lubin

(Invited)

Abstract—**This paper presents an exact analytical subdomain model of dual-stator consequent-pole permanent-magnet (DSCPPM) machines accounting for tooth-tips, which can accurately predict the armature reaction field distribution in DSCPPM machines. In the proposed subdomain model, the field domain is composed of four types of sub-regions, viz. magnets, outer/inner air gaps, slots and slot openings. The analytical expressions of vector potential in each sub-region are determined by boundary and interface conditions. In comparison to the analytically predicted results, the corresponding flux density field distributions computed by finite element (FE) method are analyzed, which confirms the excellent accuracy of the developed subdomain model.**

Index Terms—**Analytical model, armature reaction, consequent-pole, dual-stator, permanent-magnet machines, subdomain model.**

I. INTRODUCTION

DUE to increasing focus of attention on environmental and energy issues, renewable energy has attracted considerable concerns. As one of the promising new energy resources, the wind power has the advantages of reproducible and abundant resources, which has been widely investigated in academia.

The basic characteristics of direct-drive machines applied in wind power generation can be generalized as low-speed and high-torque. As the single-stator permanent magnet (PM) machine for the requirement of low-speed and high-torque usually leads to bulky volume and low power density, the dual-stator PM machines are increasingly investigated aiming at the weakness of single-stator PM machines, for reasons of preferable space utilization and higher torque/power density. A dual-stator cup-rotor PM machine was designed and analyzed in [1], which confirmed the high torque/power density of dual-stator PM machine. In [2]-[4], the vernier PM machine structure is applied in dual-stator PM machine, which further

improves the torque density and reduce the cogging torque. Very recently, a dual-stator consequent-pole PM vernier machine was proposed in [5] and it realized higher torque density with decreased consumption of PM material, which can be suitable for low-speed and high-torque direct-drive applications.

With the development of finite element method (FEM), great convenience has contributed to the design and optimization processes of PM machines, which can predict the flux density field distributions of various kinds of topologies with excellent accuracy [6]-[8]. However, due to the independent structures of inner/outer stator, more flexible design configurations of dual-stator PM machines are possible compared with single-stator PM machines. Thus, multiple variables need to be considered and optimized during the process of optimization for dual-stator PM machines, which makes the FEM quite time-consuming. Therefore, efforts should be made to investigate models which can present quick and accurate flux density predictions for complex structured machines like dual-stator PM machines. The analytical modeling is preferred for its fast calculation speed and the advantage of giving physical insights, which receives continuous attention during the development of PM machines. Thus, the target of this paper is to analytically predict the armature reaction field distributions for DSCPPM machines by subdomain model accounting for tooth-tips.

The subdomain model has been widely investigated for PM machines due to its excellent calculation accuracy, especially for the cogging torque prediction in [9]. The open-circuit subdomain model for general surfaced-mounted PM machines was studied in [10] and [11], the subdomain model for predicting the armature reaction field of general surfaced-mounted PM machines accounting for tooth-tips can be found in [12]. In addition, many other references proposed subdomain models for specific machines. An accurate subdomain model for predicting the armature reaction field of ironless brushless direct current (DC) machine was presented in [13]. An analytical method based on subdomain model using 2-D Cartesian coordinate system for calculating the armature reaction field distributions of PM linear synchronous machine was proposed in [14], which was compared and verified by 3-D FEM and experimental measured data. A subdomain model of magnetic gears with consequent-pole magnet rotors was precisely established in [15]. Besides, a subdomain model for

predicting field distribution in PM vernier machine was established in [16], an exact subdomain model for single-stator consequent-pole PM machine was proposed in [17] and a dual-rotor PM machine was investigated by subdomain model in [18], which showed its efficiency for quick electromagnetic analysis.

The structure of this paper is shown as follows. Section II explains the processes of analytical field modelling, including the governing function of vector potentials and derivation of magnetic field solution. Section III presents the analytically predicted results in the investigated DSCPPM machine, which are compared and validated by FEM. The corresponding conclusion is drawn in Section IV and detailed derivation of boundary conditions is presented in appendix.

II. ANALYTICAL FIELD MODELING

The subdomain model for the DSCPPM machine with tooth-tips is shown in Fig. 1. It should be noted that the magnets are not taken into account and considered as air (B_r=0) for region 1i in Fig. 1.

For simplicity of calculation, the following assumptions are considered: (1) infinite permeable materials for stator/rotor laminations; (2) end effects are insignificant; (3) unity relative permeability of magnet; (4) only z-direction component of magnetic vector potentials; (5) uniform current density in slot area and (6) simplified slots with radial sides as shown in Fig. 1.
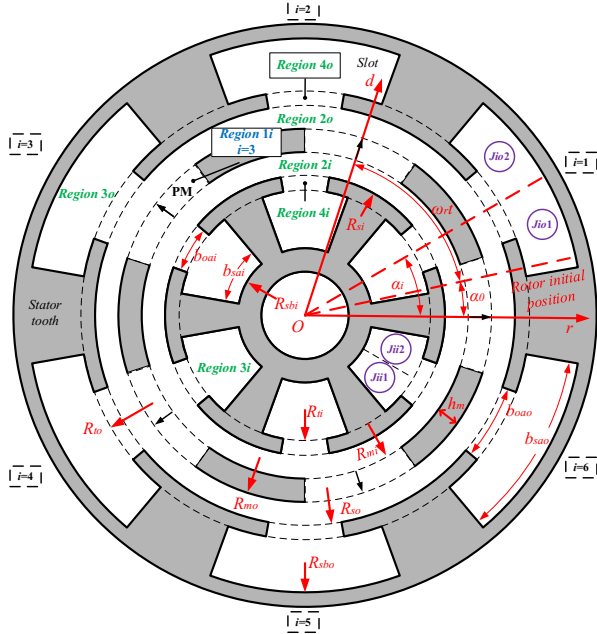

Fig. 1. Subdomain model for the DSCPPM machine with tooth-tips.

For magnetic field due to armature reaction, the magnetic vector potential A satisfies the governing function as:

$$\nabla^2 A =$$

$$\begin{cases} 0, & in\ magnet\ /\ airgap\ /\ slot\ opening \\ -\mu_0 J, & in\ slot \end{cases} \quad (1)$$

where μ_0 is the permeability of vacuum and J is the current density in the slot.

A. Field solutions in magnets

Since the vector potential in sub-region of magnets satisfies

the Laplacian function, the general solution of vector potential in the ith magnet A_{mi} can be derived and expanded into Fourier series as:

$$A_{mi} = \sum_v \left[C_{mi} \left(r / R_{mo} \right)^{F_v} + D_{mi} \left(r / R_{mi} \right)^{-F_v} \right] \cdot$$
$$\cos\left[F_v \left(\alpha - \alpha_{im} + \alpha_{mag} / 2 \right) \right] + D_m \ln r \quad (2)$$

$$F_v = vp / \alpha_r \quad (3)$$

$$\alpha_{mag} = \alpha_r \pi / p \quad (4)$$

$$\alpha_{im} = \alpha_0 + (i-1) \cdot 2\pi / p + \omega_r t \quad (5)$$

where α_r is the pole-arc to pole-pitch ratio, α_o is the initial position of rotor, ω_r is the mechanical angular speed, v is the number of spatial harmonics considered in the magnet and R_{mi}/R_{mo} are the inner/outer radii of magnet surfaces, respectively.

As the radial/circumferential flux densities can be given by

$$B_r = \frac{1}{r} \frac{\partial A}{\partial \alpha} \quad B_\alpha = -\frac{\partial A}{\partial r} \quad (6)$$

the following analytical solutions can be obtained:

$$B_{rmi} = -\sum_v (F_v / r) \cdot \left[C_{mi} \left(r / R_{mo} \right)^{F_v} + D_{mi} \left(r / R_{mi} \right)^{-F_v} \right]$$
$$\sin\left[F_v \left(\alpha - \alpha_{im} + \alpha_{mag} / 2 \right) \right] \quad (7)$$

$$B_{\alpha mi} = -\sum_v (F_v / r) \cdot \left[C_{mi} \left(r / R_{mo} \right)^{F_v} - D_{mi} \left(r / R_{mi} \right)^{-F_v} \right]$$
$$\cos\left[F_v \left(\alpha - \alpha_{im} + \alpha_{mag} / 2 \right) \right] - D_m / r \quad (8)$$

where $B_{rmi}/B_{\alpha mi}$ are the radial/circumferential flux densities in the ith magnet region.

B. Field solutions in outer/inner air-gaps and slot openings

By solving the Laplacian function shown in (1), the vector potentials in air-gaps and slot openings can be deduced as

$$A_{z2o} = \sum_{ko} \left[A_{2o} \left(r / R_{so} \right)^{ko} + B_{2o} \left(r / R_{mo} \right)^{-ko} \right]$$
$$\cdot \cos(k_o \alpha) + \sum_{ko} \left[C_{2o} \left(r / R_{so} \right)^{ko} + D_{2o} \left(r / R_{mo} \right)^{-ko} \right] \cdot \sin(k_o \alpha) \quad (9)$$

$$A_{z2i} = \sum_{ki} \left[A_{2i} \left(r / R_{mi} \right)^{ki} + B_{2i} \left(r / R_{si} \right)^{-ki} \right]$$
$$\cdot \cos(k_i \alpha) + \sum_{ki} \left[C_{2i} \left(r / R_{si} \right)^{ki} + D_{2i} \left(r / R_{mi} \right)^{-ki} \right] \cdot \sin(k_i \alpha) \quad (10)$$

$$A_{z4oi} = \sum_{mo} \left[C_{4oi} \left(r / R_{to} \right)^{F_{mo}} + D_{4oi} \left(r / R_{so} \right)^{-F_{mo}} \right]$$
$$\cdot \cos\left[F_{mo} \left(\alpha + b_{oao} / 2 - \alpha_i \right) \right] + D_o \ln r \quad (11)$$

$$A_{z4ii} = \sum_{mi} \left[C_{4ii} \left(r / R_{ti} \right)^{-F_{mi}} + D_{4ii} \left(r / R_{si} \right)^{F_{mi}} \right]$$
$$\cdot \cos\left[F_{mi} \left(\alpha + b_{oai} / 2 - \alpha_i \right) \right] + D_i \ln r \quad (12)$$

$$F_{mo} = m_o \pi / b_{oao} \quad F_{mi} = m_i \pi / b_{oai} \quad (13)$$

where A_{z2o}/A_{z2i} are the vector potentials in regions of outer/inner air-gaps, A_{z4oi}/A_{z4ii} are the vector potentials in regions of the ith outer/inner slot opening, R_{so}/R_{si}, R_{to}/R_{ti} are the radii of outer/inner stator bore and slot top, b_{oao}/b_{oai} are the outer/inner slot opening angles, k_o/k_i and m_o/m_i denote the spatial harmonic order analyzed in outer/inner air-gaps and slot openings, respectively.

Consequently, the flux density distribution can be given as

$$B_{2ro} = \left\{ -\sum_{ko} k_o \left[A_{2o} \left(r/R_{so} \right)^{ko} + B_{2o} \left(r/R_{mo} \right)^{-ko} \right] \sin(k_o \alpha) \right.$$
$$\left. + \sum_{ko} k_o \left[C_{2o} \left(r/R_{so} \right)^{ko} + D_{2o} \left(r/R_{mo} \right)^{-ko} \right] \cos(k_o \alpha) \right\} / r \quad (14)$$

$$B_{2\alpha o} = \left\{ -\sum_{ko} k_o \left[A_{2o} \left(r/R_{so} \right)^{ko} - B_{2o} \left(r/R_{mo} \right)^{-ko} \right] \cos(k_o \alpha) \right.$$
$$\left. - \sum_{ko} k_o \left[C_{2o} \left(r/R_{so} \right)^{ko} - D_{2o} \left(r/R_{mo} \right)^{-ko} \right] \sin(k_o \alpha) \right\} / r \quad (15)$$

$$B_{2ri} = \left\{ -\sum_{ki} k_i \left[A_{2i} \left(r/R_{mi} \right)^{ki} + B_{2i} \left(r/R_{si} \right)^{-ki} \right] \sin(k_i \alpha) \right.$$
$$\left. + \sum_{ki} k_i \left[C_{2i} \left(r/R_{mi} \right)^{ki} + D_{2i} \left(r/R_{si} \right)^{-ki} \right] \cos(k_i \alpha) \right\} / r \quad (16)$$

$$B_{2\alpha i} = \left\{ -\sum_{ki} k_i \left[A_{2i} \left(r/R_{mi} \right)^{ki} - B_{2i} \left(r/R_{si} \right)^{-ki} \right] \cos(k_i \alpha) \right.$$
$$\left. - \sum_{ki} k_i \left[C_{2i} \left(r/R_{mi} \right)^{ki} - D_{2i} \left(r/R_{si} \right)^{-ki} \right] \sin(k_i \alpha) \right\} / r \quad (17)$$

$$B_{r4oi} = -(1/r) \sum_{mo} F_{mo} \left[C_{4oi} \left(r/R_{to} \right)^{F_{mo}} + \right.$$
$$\left. D_{4oi} \left(r/R_{so} \right)^{-F_{mo}} \right] \sin \left[F_{mo} \left(\alpha + b_{oao} / 2 - \alpha_i \right) \right] \quad (18)$$

$$B_{\alpha 4oi} = -(D_o/r) - (1/r) \sum_{mo} F_{mo} \left[C_{4oi} \left(r/R_{to} \right)^{F_{mo}} - \right.$$
$$\left. D_{4oi} \left(r/R_{so} \right)^{-F_{mo}} \right] \cos \left[F_{mo} \left(\alpha + b_{oao} / 2 - \alpha_i \right) \right] \quad (19)$$

$$B_{r4ii} = -(1/r) \sum_{mi} F_{mi} \left[C_{4ii} \left(r/R_{ti} \right)^{-F_{mi}} + \right.$$
$$\left. D_{4ii} \left(r/R_{si} \right)^{F_{mi}} \right] \sin \left[F_{mi} \left(\alpha + b_{oai} / 2 - \alpha_i \right) \right] \quad (20)$$

$$B_{\alpha 4ii} = -(D_i/r) - (1/r) \sum_{mi} F_{mi} \left[-C_{4ii} \left(r/R_{ti} \right)^{-F_{mi}} + \right.$$
$$\left. D_{4ii} \left(r/R_{si} \right)^{F_{mi}} \right] \cos \left[F_{mi} \left(\alpha + b_{oai} / 2 - \alpha_i \right) \right] \quad (21)$$

C. Field solutions in outer/inner slots

For armature reaction field distribution, the vector potential in slots satisfy the Possion function shown in (1). Fig. 2 shows the winding configuration and current density function in slots, respectively. The current density can be written as

$$J = J_{i0} + \sum_n J_{in} \cos[E_n(\alpha + b_{sa}/2 - \alpha_i)] \quad (22)$$

$$J_{i0} = (J_{i1} + J_{i2})/2 \quad (23)$$

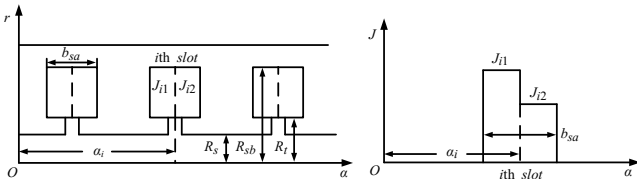$$J_{in} = (2/n\pi)(J_{i1} - J_{i2}) \sin(n\pi/2) \quad (24)$$

Fig. 2. Winding configuration and current density function.

Thus, the corresponding general solutions for vector potentials A_{z3oi}/A_{z3ii} in outer/inner slots can be deduced as:

$$A_{z3oi} = \mu_0 J_{io0}(2R_{sbo}^2 \ln r - r^2)/4 + \sum_{no} \left\{ D_{3oi} [G_3 \left(r/R_{sbo} \right)^{E_{no}} \right.$$
$$\left. + \left(r/R_{to} \right)^{-E_{no}}] + \mu_0 J_{ino} [r^2 - 2R_{sbo}^2 \left(r/R_{sbo} \right)^{E_{no}} / E_{no}] \right.$$
$$\left. /(E_{no}^2 - 4) \right\} \cos \left[E_{no} \left(\alpha + b_{sao} / 2 - \alpha_i \right) \right] \quad (25)$$

$$A_{z3ii} = \mu_0 J_{ii0}(2R_{sbi}^2 \ln r - r^2)/4 + \sum_{ni} \left\{ D_{3ii} [G_{3i} \left(r/R_{sbi} \right)^{-E_{ni}} \right.$$
$$\left. + \left(r/R_{ti} \right)^{E_{ni}}] + \mu_0 J_{ini} [r^2 + 2R_{sbi}^2 \left(r/R_{sbi} \right)^{-E_{ni}} / E_{ni}] \right.$$
$$\left. /(E_{ni}^2 - 4) \right\} \cos \left[E_{ni} \left(\alpha + b_{sai} / 2 - \alpha_i \right) \right] \quad (26)$$

$$E_{no} = n_o \pi / b_{sao} \qquad E_{ni} = n_i \pi / b_{sai} \quad (27)$$

$$G_3 = \left(R_{to} / R_{sbo} \right)^{E_{no}} \qquad G_{3i} = \left(R_{sbi} / R_{ti} \right)^{E_{ni}} \quad (28)$$

where R_{sbo}/R_{sbi} are the radii of outer/inner slot bottoms and n_o/n_i denote the spatial harmonic order analyzed in outer/inner slots.

Therefore, the radial/circumferential flux densities in outer/inner slots can be deduced as

$$B_{r3oi} = -\sum_{no} \left\{ E_{no} D_{3oi} [G_3 (r/R_{sbo})^{E_{no}} + (r/R_{to})^{-E_{no}}]/r + \mu_0 J_{ino} \right.$$
$$\left. [E_{no} r - 2R_{sbo} (r/R_{sbo})^{E_{no}-1}]/(E_{no}^2 - 4) \right\} \sin \left[E_{no} \left(\alpha + b_{sao} / 2 - \alpha_i \right) \right] \quad (29)$$

$$B_{r3ii} = -\sum_{ni} \left\{ E_{ni} D_{3ii} [G_{3i} (r/R_{sbi})^{-E_{ni}} + (r/R_{ti})^{E_{ni}}]/r + \mu_0 J_{ini} \right.$$
$$\left. [E_{ni} r + 2R_{sbi} (r/R_{sbi})^{-E_{ni}-1}]/(E_{ni}^2 - 4) \right\} \sin \left[E_{ni} \left(\alpha + b_{sai} / 2 - \alpha_i \right) \right] \quad (30)$$

$$B_{\alpha 3oi} = -\mu_0 J_{io0}(R_{sbo}^2 / r - r)/2 - \sum_{no} \left\{ E_{no} D_{3oi} [G_3 (r/R_{sbo})^{E_{no}} \right.$$
$$\left. - (r/R_{to})^{-E_{no}}]/r + 2\mu_0 J_{ino} [r - R_{sbo} (r/R_{sbo})^{E_{no}-1}] \right.$$
$$\left. /(E_{no}^2 - 4) \right\} \cos \left[E_{no} \left(\alpha + b_{sao} / 2 - \alpha_i \right) \right] \quad (31)$$

$$B_{\alpha 3ii} = -\mu_0 J_{ii0}(R_{sbi}^2 / r - r)/2 - \sum_{ni} \left\{ E_{ni} D_{3ii} [(r/R_{ti})^{E_{ni}} - \right.$$
$$\left. G_{3i} (r/R_{sbi})^{-E_{ni}}]/r + 2\mu_0 J_{ini} [r - R_{sbi} (r/R_{sbi})^{-E_{ni}-1}] \right.$$
$$\left. /(E_{ni}^2 - 4) \right\} \cos \left[E_{ni} \left(\alpha + b_{sai} / 2 - \alpha_i \right) \right] \quad (32)$$

The undermined coefficients C_{mi}/D_{mi}, A_{2o}-D_{2o}/A_{2i}-D_{2i}, C_{4oi}/C_{4ii}, D_{3oi}/D_{3ii}, D_{4oi}/D_{4ii}, D_m, D_o/D_i are calculated by applying the boundary conditions between sub-regions. The detailed computation processes of the boundary conditions are given in the appendix.

III. RESULTS AND VALIDATION

In this section, the proposed 2-D subdomain model is applied to predict the flux density distribution in all sub-regions. An example of 12-stator-slot/5-rotor-iron piece DSCPPM machine is investigated, its main design parameters are listed in Table I. Besides, the FE model is established for validation.

Fig. 3-5 show the comparisons of flux density distributions computed using FE and analytical methods in outer air-gap, slots and slot openings, respectively. The results show that the analytically predicted flux densities in outer part of the machine have excellent agreement with FE results in both circumferential and radial directions.

TABLE I
DESIGN PARAMETERS OF DUAL-STATOR MACHINE

Parameter	Dual-stator machine	
Stator outer radius (mm)	100	
Stator inner radius (mm)	28	
Air-gap length outer/inner(mm)	1.5	1.5
Magnet thickness (mm)	5	
Stator bore (mm)	65	57
Tooth-tip height outer/inner(mm)	4	4
Active length (mm)	50	
Slot width angle outer/inner(deg.)	20	20

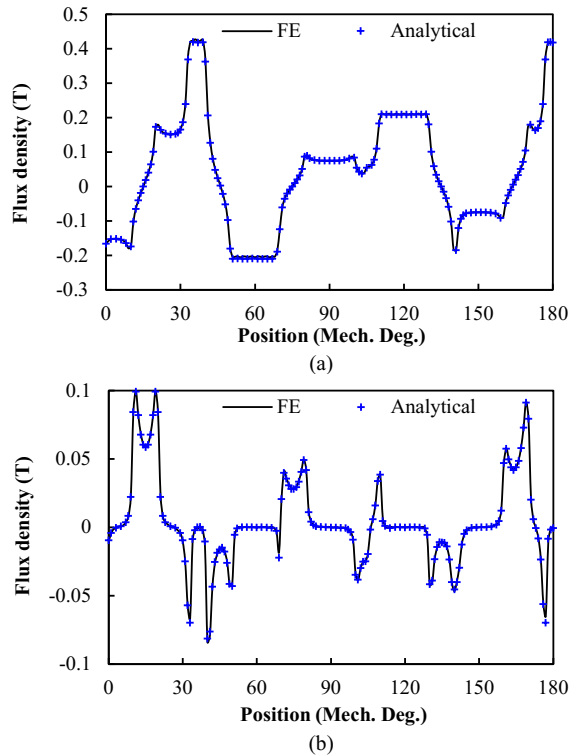| Slot opening angle outer/inner(deg.)	10	5
Initial position of rotor(deg.)	15	
Pole arc to pitch ratio	1	
Number of turns/coil	50	
Rated speed (rpm)	600	
Number of pole pairs/slots	5/12	
Rated current(A)	10 (A_{peak})	

Fig. 3. Flux density predictions for (a) radial and (b) circumferential components at mid outer air-gap using FE and analytical approaches.
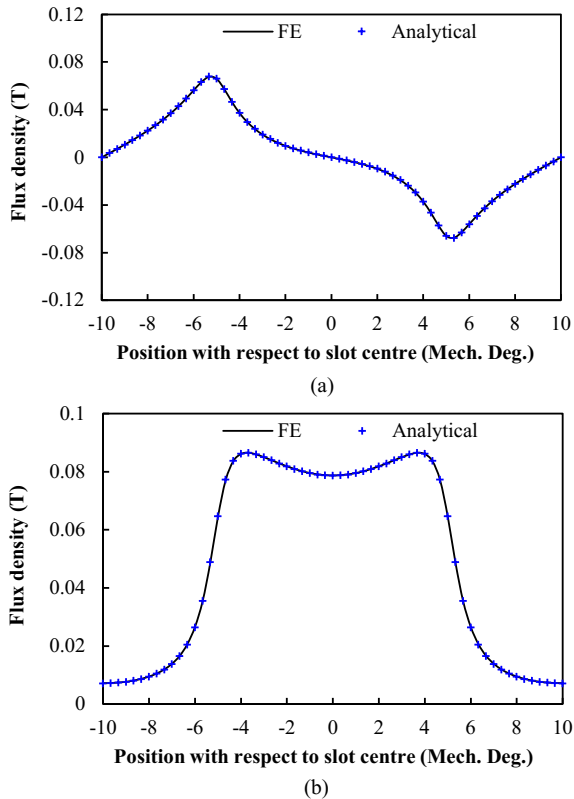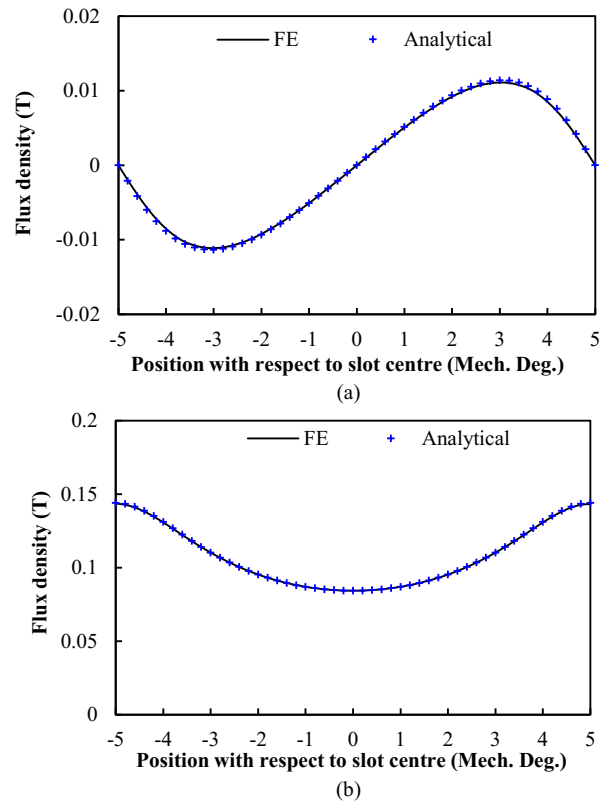

Fig. 4. Flux density predictions for (a) radial and (b) circumferential components at the 1st slot at $r=R_{to}+1$ mm using FE and analytical approaches.

Fig. 5. Flux density predictions for (a) radial and (b) circumferential components at the 1st mid outer slot opening using FE and analytical approaches.

Fig. 6-8 show the comparisons of flux density distributions computed using FE and analytical methods in the inner stator part. Equally, the analytically predicted flux densities for the inner part match perfectly with the FE results.
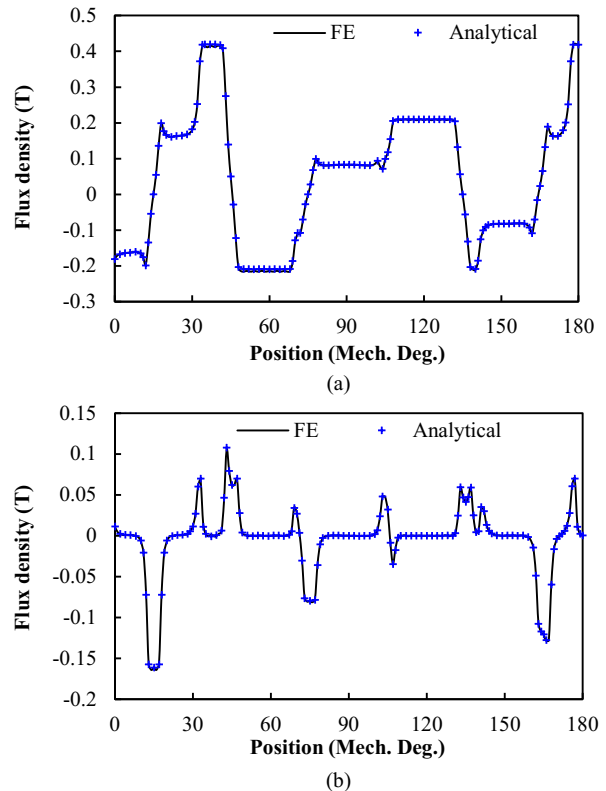

Fig. 6. Flux density predictions for (a) radial and (b) circumferential components at mid inner air-gap using FE and analytical approaches.
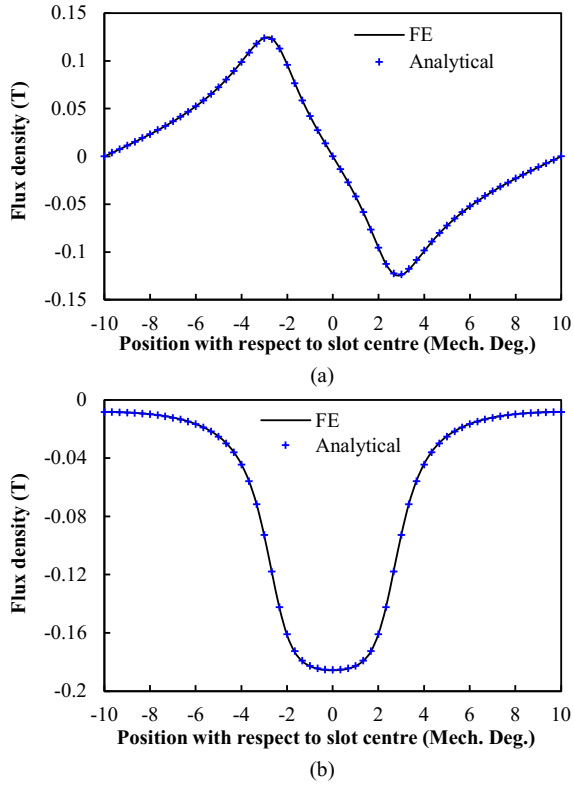
(a)

(b)

Fig. 7. Flux density predictions for (a) radial and (b) circumferential components at the 1st slot at $r=R_{ti}-1$ mm using FE and analytical approaches.
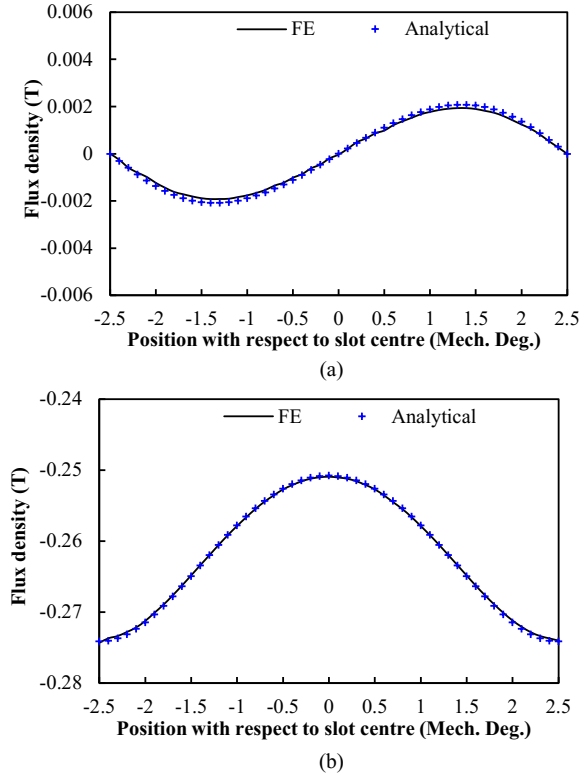

(a)

(b)

Fig. 8. Flux density predictions for (a) radial and (b) circumferential components at the 1st mid inner slot opening region using FE and analytical approaches.

IV. CONCLUSION

An exact analytical subdomain model considering tooth-tip

effect for predicting armature reaction field in DSCPPM machine has been presented in this paper. Based on the proposed subdomain model, the flux density distributions in magnets, outer/inner air-gaps, slots and slot openings can be calculated quickly, which can be beneficial in the process of initial design and optimization for DSCPPM machines. In comparison with the analytical predictions, the 2-D FE model has been established and analyzed. The proposed subdomain model shows its excellent accuracy in predicting the armature field distributions in all sub-regions, which is valuable for predicting other electromagnetic properties, such as electromagnetic torque, winding inductance, risk of irreversible demagnetization and unbalanced magnetic force, etc., which will be discussed and published in another paper.

V. APPENDIX

On the boundary between sub-regions I and II, the continuity of magnetic intensity and vector potential can be expressed as

$$H_{I\alpha} = H_{II\alpha} \quad and \quad A_I = A_{II} \tag{33}$$

Thus, the boundary conditions between different subdomains are deduced and analyzed in this section.

A. Boundary between outer/inner slots and slot openings

The boundary conditions between outer slot openings and slots at $r=R_{to}$ are investigated, it can be deduced from (19) that

$$B_{\alpha 4oi}\big|_{r=Rto} = B_{4o\alpha 0} + \sum_{mo} B_{4o\alpha m} \cos\left[F_{mo}\left(\alpha + b_{oao}/2 - \alpha_i\right)\right]$$
$$= B_0 + \sum_{no} B_n \cos\left[E_{no}\left(\alpha + b_{sao}/2 - \alpha_i\right)\right] \tag{34}$$

where

$$B_{4o\alpha 0} = -D_o/R_{to} \quad B_{4o\alpha m} = -F_{mo}\left[C_{4oi} - D_{4oi}G_4\right]/R_{to} \tag{35}$$
$$B_0 = B_{4o\alpha 0}b_{oao}/b_{sao} \quad B_n = B_{4o\alpha 0}\gamma_0 + \sum_{mo} B_{4o\alpha m}\gamma_o \tag{36}$$

where

$$\gamma_0(n_o) = 4\cos(n_o\pi/2)\sin(E_{no}b_{oao}/2)/(n_o\pi) \tag{37}$$
$$\gamma_o(m_o,n_o) = -2E_{no}\cdot\left[\sin[E_{no}(b_{sao}+b_{oao})/2]\cdot\cos(m_o\pi)\right.$$
$$\left. - \sin[E_{no}(b_{sao}-b_{oao})/2]\right]/\left[b_{sao}(F_{mo}^2 - E_{no}^2)\right] \tag{38}$$

The circumferential flux density $B_{\alpha 3oi}$ at $r=R_{to}$ can also be acquired as

$$B_{\alpha 3oi}\big|_{r=Rto} = B_{3o\alpha 0} + \sum_{no} B_{3o\alpha n}\cos\left[E_n\left(\alpha + b_{sao}/2 - \alpha_i\right)\right] \tag{39}$$

where

$$B_{3o\alpha 0} = -\mu_0 J_{i0}\left(R_{sbo}^2 - R_{to}^2\right)/2R_{to} \tag{40}$$
$$B_{3o\alpha n} = -[E_{no}D_{3oi}(G_3^2 - 1) + 2\mu_0 J_{ino}(R_{to}^2 - R_{sbo}^2 G_3)/(E_{no}^2 - 4)]/R_{to} \tag{41}$$

According to the continuity of flux density, the relational formulas can be given as

$$B_{3o\alpha 0} = B_{4o\alpha 0}b_{oao}/b_{sao} \tag{42}$$
$$B_{3o\alpha n} = B_{4o\alpha 0}\gamma_0 + \sum_{mo} B_{4o\alpha m}\gamma_o \tag{43}$$
$$D_o = \mu_0 J_{i0o}b_{sao}(R_{sbo}^2 - R_{to}^2)/(2b_{oao}) \tag{44}$$

Based on (25), the vector potential A_{z3oi} in the ith outer slot at $r=R_{to}$ can be obtained and reformed as

$$A_t = A_{z3oi}|_{r=R_{to}}$$

$$= A_{3o0} + \sum_{no} A_{3on} \cos[E_{no}(\alpha + b_{sao}/2 - \alpha_i)] \quad (45)$$

$$= A_{3t0} + \sum_{mo} A_{3tm} \cos[F_{mo}(\alpha + b_{oao}/2 - \alpha_i)]$$

where

$$A_{3o0} = \mu_0 J_{i0}(2R_{sbo}^2 \ln R_{to} - R_{to}^2)/4 \quad (46)$$

$$A_{3on} = D_{3oi}(G_3^2 + 1) + \mu_0 J_{ino}(R_{to}^2 - 2R_{sbo}^2 G_3/E_{no})/(E_{no}^2 - 4) \quad (47)$$

$$A_{3t0} = \sum_{no} A_{3on}\zeta_0 + \mu_0 J_{i0}(2R_{sbo}^2 \ln R_{to} - R_{to}^2)/4 \quad (48)$$

$$A_{3tm} = \sum_{no} A_{3on}\zeta_o \quad (49)$$

where

$$\zeta_0(n_o) = (b_{sao}/2b_{oao})\gamma_0(n_o) \quad (50)$$

$$\zeta_o(m_o, n_o) = (b_{sao}/b_{oao})\gamma_o(m_o, n_o) \quad (51)$$

Meanwhile, it can be derived by (11) as

$$A_{z4oi}|_{r=R_{to}} = D_o \ln R_{to} +$$

$$\sum_{mo}[C_{4oi} + D_{4oi}G_4]\cos[F_{mo}(\alpha + b_{oao}/2 - \alpha_i)] \quad (52)$$

Thus, the following relational formulas can be obtained according to the continuity of vector potential as

$$C_{4oi} + D_{4oi}G_4 = \sum_{no} A_{3on}\zeta_o \quad (53)$$

Equally, the boundary conditions between inner slot and slot opening are investigated and rearranged as

$$B_{3i\alpha n} = B_{4i\alpha 0}\gamma_{i0} + \sum_{mi} B_{4i\alpha m}\gamma_i \quad (54)$$

$$C_{4ii} + D_{4ii}G_4 = \sum_{ni} A_{3in}\zeta_i \quad (55)$$

where

$$B_{3i\alpha n} = -[E_{ni}D_{3ii}(1 - G_{3i}^2) + 2\mu_0 J_{ini}(R_{ti}^2 - R_{sbi}^2 G_{3i})/(E_{ni}^2 - 4)]/R_{ti} \quad (56)$$

$$B_{4i\alpha 0} = -D_i/R_{ti} \quad B_{4i\alpha m} = -F_{mi}[D_{4ii}G_{4i} - C_{4ii}]/R_{ti} \quad (57)$$

$$D_i = \mu_0 J_{i0i}b_{sai}(R_{sbi}^2 - R_{ti}^2)/(2b_{oai}) \quad (58)$$

$$\gamma_{i0}(n_i) = 4\cos(n_i\pi/2)\sin(E_{ni}b_{oai}/2)/(n_i\pi) \quad (59)$$

$$\gamma_i(m_i, n_i) = -2E_{ni} \cdot [\sin[E_{ni}(b_{sai} + b_{oai})/2] \cdot \cos(m_i\pi)$$

$$- \sin[E_{ni}(b_{sai} - b_{oai})/2]]/[b_{sai}(F_{mi}^2 - E_{ni}^2)] \quad (60)$$

where

$$A_{3in} = D_{3ii}(G_{3i}^2 + 1) + \mu_0 J_{ini}(R_{ti}^2 - 2R_{sbi}^2 G_{3i}/E_{ni})/(E_{ni}^2 - 4) \quad (61)$$

$$\zeta_i(m_i, n_i) = (b_{sai}/b_{oai})\gamma_i(m_i, n_i) \quad (62)$$

B. Boundary between outer/inner slot openings and air-gaps

The boundary between outer/inner slot openings and air-gaps can be applied in a similar way. As the circumferential flux density is continuous at $r=R_{so}$, the following expressions can be acquired from (19)

$$B_{\alpha 4oi}|_{r=R_{so}} = B_{i\alpha 0} + \sum_{mo} B_{i\alpha m} \cos[F_{mo}(\alpha + b_{oao}/2 - \alpha_i)]$$

$$= \sum_{ko}[C_s \cos(k_o\alpha) + D_s \cos(k_o\alpha)] \quad (63)$$

where

$$B_{i\alpha 0} = -D_o/R_{so} \quad (64)$$

$$B_{i\alpha m} = -F_{mo}[C_{4i}G_4 - D_{4i}]/R_{so} \quad (65)$$

$$C_s = \sum_i \sum_{mo} B_{i\alpha m}\eta_{io} + \sum_i B_{i\alpha 0}\eta_{io0} \quad (66)$$

$$D_s = \sum_i \sum_{mo} B_{i\alpha m}\xi_{io} + \sum_i B_{i\alpha 0}\eta_{io0} \quad (67)$$

where

$$\eta_{io}(m_o, k_o) = -k_o \cdot [\sin(k_o\alpha_i + k_o b_{oao}/2) \cdot \cos(m_o\pi)$$

$$- \sin(k_o\alpha_i - k_o b_{oao}/2)]/[\pi(F_{mo}^2 - k_o^2)] \quad (68)$$

$$\xi_{io}(m_o, k_o) = k_o \cdot [\cos(k_o\alpha_i + k_o b_{oao}/2) \cdot \cos(m_o\pi)$$

$$- \cos(k_o\alpha_i - k_o b_{oao}/2)]/[\pi(F_{mo}^2 - k_o^2)] \quad (69)$$

$$\eta_{io0}(k_o) = 2\cos(k_o\alpha_i)\sin(k_o b_{oao}/2)/(k_o\pi) \quad (70)$$

$$\xi_{io0}(k_o) = 2\sin(k_o\alpha_i)\sin(k_o b_{oao}/2)/(k_o\pi) \quad (71)$$

In the same manner, it can be given from (15) as

$$B_{2\alpha o}|_{r=R_{so}} = -(1/R_{so})\sum_{ko}k_o(A_{2o} - B_{2o}G_2)\cos(k_o\alpha)$$

$$- (1/R_{so})\sum_{ko}k_o(C_{2o} - D_{2o}G_2)\sin(k_o\alpha) \quad (72)$$

Combining (63) and (72), the relational formulas are obtained as

$$k_o(A_{2o} - B_{2o}G_2) = \sum_i \sum_{mo} F_{mo}[C_{4oi}G_4 - D_{4oi}]\eta_{io} + \sum_i \eta_{io0}D_o \quad (73)$$

$$k_o(C_{2o} - D_{2o}G_2) = \sum_i \sum_{mo} F_{mo}[C_{4oi}G_4 - D_{4oi}]\xi_{io} + \sum_i \xi_{io0}D_o \quad (74)$$

The vector potential A_{z2o} at $r=R_{so}$ can be given as

$$A_s = A_{z2o}|_{r=R_{so}} = \sum_{ko}[A'_{2c}\cos(k_o\alpha) + A'_{2s}\sin(k_o\alpha)]$$

$$= \sum_{mo} A_{oi}\cos[F_{mo}(\alpha + b_{oao}/2 - \alpha_i)] + A_{oi0} \quad (75)$$

where

$$A'_{2c} = A_{2o} + B_{2o}G_2 \quad A'_{2s} = C_{2o} + D_{2o}G_2 \quad (76)$$

$$A_{oi} = \sum_{ko}(A'_{2c}\sigma_{io} + A'_{2s}\tau_{io}) \quad A_{oi0} = \sum_{ko}(A'_{2c}\sigma_{io0} + A'_{2s}\tau_{io0}) \quad (77)$$

where

$$\sigma_{io} = 2\pi\eta_{io}/b_{oao} \quad \tau_{io} = 2\pi\xi_{io}/b_{oao} \quad (78)$$

$$\sigma_{io0} = \pi\eta_{io0}/b_{oao} \quad \tau_{io0} = \pi\xi_{io0}/b_{oao} \quad (79)$$

The vector potential A_{z4oi} in the ith outer slot opening at $r=R_{so}$ can be calculated as

$$A_s = A_{z4oi}|_{r=R_{so}} = D_o \ln R_{so} + \sum_{mo}[C_{4oi}G_4 + D_{4oi}]$$

$$\cos[F_{mo}(\alpha + b_{oao}/2 - \alpha_i)] \quad (80)$$

According to the continuity of vector potential, the following relational formulas can be derived as

$$\sum_{ko}[A'_{2c}\sigma_{io0} + A'_{2s}\tau_{io0}] = D_o \ln R_{so} \quad (81)$$

$$C_{4oi}G_4 + D_{4oi} = \sum_{ko}(A'_{2c}\sigma_{io} + A'_{2s}\tau_{io}) \quad (82)$$

Similarly, the boundary conditions between inner slot openings and air-gaps are deduced, which can be rearranged as

$$k_i(A_{2i}G_{2i} - B_{2i}) = \sum_i \sum_{mi} F_{mi}[D_{4ii} - C_{4ii}G_{4i}]\eta_{ii} + \sum_i \eta_{ii0}D_i \quad (83)$$

$$k_i(C_{2i}G_{2i} - D_{2i}) = \sum_i \sum_{mi} F_{mi}[D_{4ii} - C_{4ii}G_{4i}]\xi_{ii} + \sum_i \xi_{ii0}D_i \quad (84)$$

$$C_{4ii}G_{4i} + D_{4ii} = \sum_{ki}(A'_{2ci}\sigma_{ii} + A'_{2si}\tau_{ii}) \quad (85)$$

$$\sum_{ki}[A'_{2ci}\sigma_{ii0} + A'_{2si}\tau_{ii0}] = D_i \ln R_{si} \quad (86)$$

where

ZHU et al: SUBDOMAIN MODEL FOR PREDICTING ARMATURE REACTION FIELD OF DUAL-STATOR CONSEQUENT-POLE PM MACHINES ACCOUNTING FOR TOOTH-TIPS

149

$$G_4 = (R_{so}/R_{to})^{F_{mo}} \quad G_{4i} = (R_{ti}/R_{si})^{F_{mi}} \tag{87}$$

$$\eta_{ii}(m_i,k_i) = -k_i \cdot \big[\sin(k_i\alpha_i + k_i b_{oai}/2) \cdot \cos(m_i\pi)$$
$$- \sin(k_i\alpha_i - k_i b_{oai}/2) \big] / [\pi(F_{mi}^2 - k_i^2)] \tag{88}$$

$$\xi_{ii}(m_i,k_i) = k_i \big[\cos(k_i\alpha_i + k_i b_{oai}/2) \cdot \cos(m_i\pi)$$
$$- \cos(k_i\alpha_i - k_i b_{oai}/2) \big] / [\pi(F_{mi}^2 - k_i^2)] \tag{89}$$

$$\eta_{ii0}(k_i) = 2\cos(k_i\alpha_i)\sin(k_i b_{oai}/2)/(k_i\pi) \tag{90}$$

$$\xi_{ii0}(k_i) = 2\sin(k_i\alpha_i)\sin(k_i b_{oai}/2)/(k_i\pi) \tag{91}$$

where

$$A'_{2ci} = A_{2i}G_{2i} + B_{2i} \quad A'_{2si} = C_{2i}G_{2i} + D_{2i} \tag{92}$$

$$\sigma_{ii} = 2\pi\eta_{ii}/b_{oai} \quad \tau_{ii} = 2\pi\xi_{ii}/b_{oai} \tag{93}$$

$$\sigma_{ii0} = \pi\eta_{ii0}/b_{oai} \quad \tau_{ii0} = \pi\xi_{ii0}/b_{oai} \tag{94}$$

C. Boundary between PM and inner/outer air-gaps

For boundary between PM and outer air-gap, the circumferential component of magnetic intensity is continuous at $r=R_{mo}$, which can be represented as:

$$H_{\alpha mi} = B_{\alpha mi}/\mu_0$$
$$H_{2\alpha o} = B_{2\alpha o}/\mu_0 \tag{95}$$

Based on the magnetic field solution in the former section, it can be obtained from (8) as

$$B_{\alpha mi}\big|_{r=R_{mo}} = \sum_v B_{i\alpha v}\cos\big[F_v(\alpha - \alpha_{im} + \alpha_{mag}/2)\big] - D_m/R_{mo}$$
$$= \sum_{ko}[C_{mo}\cos(k_o\alpha) + D_{mo}\sin(k_o\alpha)] - D_m/R_{mo} \tag{96}$$

where

$$B_{i\alpha v} = -\frac{F_v}{R_{mo}} \cdot [C_{mi} - D_{mi}G_1] \tag{97}$$

In the same way, it can be obtained from (15) as

$$B_{2\alpha o}\big|_{r=R_{mo}} = -(1/R_{mo})\sum_{ko} k_o(A_{2o}G_2 - B_{2o})\cdot\cos(k_o\alpha)$$
$$-(1/R_{mo})\sum_{ko} k_o(C_{2o}G_2 - D_{2o})\cdot\sin(k_o\alpha) \tag{98}$$

where

$$G_1 = (R_{mi}/R_{mo})^{F_v} \quad G_2 = (R_{mo}/R_{so})^{ko} \tag{99}$$

$$C_{mo} = \sum_i \sum_v B_{i\alpha v}\eta_{mio} \quad D_{mo} = \sum_i \sum_v B_{i\alpha v}\xi_{mio} \tag{100}$$

$$\eta_{mio}(v,k_o) = -k_o \cdot \big[\sin(k_o\alpha_{im} + k_o\alpha_{mag}/2) \cdot \cos(v\pi)$$
$$- \sin(k_o\alpha_{im} - k_o\alpha_{mag}/2) \big] / [\pi(F_v^2 - k_o^2)] \tag{101}$$

$$\xi_{mio}(v,k_o) = k_o \cdot \big[\cos(k_o\alpha_{im} + k_o\alpha_{mag}/2) \cdot \cos(v\pi)$$
$$- \cos(k_o\alpha_{im} - k_o\alpha_{mag}/2) \big] / [\pi(F_v^2 - k_o^2)] \tag{102}$$

According to the continuity of magnetic intensity shown as (33), the following expressions can be obtained as

$$D_m = 0 \tag{103}$$

$$k_o(A_{2o}G_2 - B_{2o}) = \sum_i \sum_v F_v \cdot (C_{mi} - D_{mi}G_1)\eta_{mio} \tag{104}$$

$$k_o(C_{2o}G_2 - D_{2o}) = \sum_i \sum_v F_v \cdot (C_{mi} - D_{mi}G_1)\xi_{mio} \tag{105}$$

The vector potential at outer magnet surface can be obtained

as

$$A_{z2o}\big|_{r=R_{mo}} = \sum_{ko}[A_{2c}\cos(k_o\alpha) + A_{2s}\sin(k_o\alpha)]$$
$$= \sum_v \sum_{ko}(A_{2c}\sigma_{mio} + A_{2s}\tau_{mio})\cos\big[F_v(\alpha - \alpha_{im} + \alpha_{mag}/2)\big] \tag{106}$$

where

$$A_{2c} = A_{2o}G_2 + B_{2o} \quad A_{2s} = C_{2o}G_2 + D_{2o} \tag{107}$$

Equally, it can be deduced from (2) as

$$A_{mi}\big|_{r=R_{mo}} = \sum_v (C_{mi} + D_{mi}G_1)\cos[F_v(\alpha - \alpha_{im} + \alpha_{mag}/2)] \tag{108}$$

According to the continuity of vector potential, it can be arranged as

$$\sum_{ko}(A_{2c}\sigma_{mio} + A_{2s}\tau_{mio}) = C_{mi} + D_{mi}G_1 \tag{109}$$

where

$$\sigma_{mio} = (2\pi/\alpha_{mag})\eta_{mio} \quad \tau_{mio} = (2\pi/\alpha_{mag})\xi_{mio} \tag{110}$$

Similarly, the boundary conditions between PM and inner air-gap are analyzed, which can be rearranged as

$$k_i(A_{2i} - B_{2i}G_{2i}) = \sum_i \sum_v F_v \cdot (C_{mi}G_1 - D_{mi})\eta_{mii} \tag{111}$$

$$k_i(C_{2i} - D_{2i}G_{2i}) = \sum_i \sum_v F_v \cdot (C_{mi}G_1 - D_{mi})\xi_{mii} \tag{112}$$

$$\sum_{ki}(A_{2ci}\sigma_{mii} + A_{2si}\tau_{mii}) = C_{mi}G_1 + D_{mi} \tag{113}$$

where

$$A_{2ci} = A_{2i} + B_{2i}G_{2i} \quad A_{2si} = C_{2i} + D_{2i}G_{2i} \tag{114}$$

$$G_{2i} = (R_{si}/R_{mi})^{ki} \tag{115}$$

$$\eta_{mii}(v,k_i) = -k_i \cdot \big[\sin(k_i\alpha_{im} + k_i\alpha_{mag}/2) \cdot \cos(v\pi)$$
$$- \sin(k_i\alpha_{im} - k_i\alpha_{mag}/2) \big] / [\pi(F_v^2 - k_i^2)] \tag{116}$$

$$\xi_{mii}(v,k_i) = k_i \cdot \big[\cos(k_i\alpha_{im} + k_i\alpha_{mag}/2) \cdot \cos(v\pi)$$
$$- \cos(k_i\alpha_{im} - k_i\alpha_{mag}/2) \big] / [\pi(F_v^2 - k_i^2)] \tag{117}$$

$$\sigma_{mii} = (2\pi/\alpha_{mag})\eta_{mii} \quad \tau_{mii} = (2\pi/\alpha_{mag})\xi_{mii} \tag{118}$$

REFERENCES

[1] S. Niu, K. T. Chau, J. Z. Jiang, and C. Liu, "Design and control of a new double-stator cup-rotor permanent-magnet machine for wind power generation," *IEEE Trans. Magn.*, vol. 43, no. 6, pp. 2501-2503, Jun. 2007.

[2] S. Niu, S. L. Ho, and W. N. Fu, "A novel direct-drive dual-structure permanent magnet machine," *IEEE Trans. Magn.*, vol. 46, no. 6, pp. 2036-2039, Jun. 2010.

[3] F. Zhao, T. A. Lipo, and B. Kwon, "A novel dual-stator axial-flux spoke-type permanent magnet vernier machine for direct-drive applications," *IEEE Trans. Magn.*, vol. 50, no. 11, pp. 1-4, Nov. 2014.

[4] D. Li, R. Qu, W. Xu, J. Li, and T. A. Lipo, "Design procedure of dual-stator spoke-array vernier permanent-magnet machines," *IEEE Trans. Ind. Appl.*, vol. 51, no. 4, pp. 2972-2983, July-Aug. 2015.

[5] N. Baloch, B. Kwon, and Y. Gao, "Low-cost high-torque-density dual-stator consequent-pole permanent magnet vernier machine," *IEEE Trans. Magn.*, vol. 54, no. 11, pp. 1-5, Nov. 2018.

[6] X. Liu, H. Lin, Z. Q. Zhu, C. Yang, S. Fang, and J. Guo, "A novel dual-stator hybrid excited synchronous wind generator," *IEEE Trans. Ind. Appl.*, vol. 45, no. 3, pp. 947-953, May-June 2009.

[7] M. Aydin, S. Huang, and T. A. Lipo, "Design, analysis, and control of a hybrid field-controlled axial-flux permanent-magnet motor," *IEEE Trans. Ind. Electron.*, vol. 57, no. 1, pp. 78-87, Jan. 2010.

[8] J. Bai, P. Zheng, C. Tong, Z. Song, and Q. Zhao, "Characteristic analysis and verification of the magnetic-field-modulated brushless double-rotor machine," *IEEE Trans. Ind. Electron.*, vol. 62, no. 7, pp. 4023-4033, Jul.

2015.

[9]   L. J. Wu, Z. Q. Zhu, D. A. Staton, M. Popescu, and D. Hawkins, "Comparison of analytical models of cogging torque in surface-mounted PM machines," *IEEE Trans. Ind. Electron.*, vol. 59, no. 6, pp. 2414-2425, Jun. 2012.

[10] Z. J. Liu and J. T. Li, "Accurate prediction of magnetic field and magnetic forces in permanent magnet motors using an analytical solution," *IEEE Trans. Energy Convers.*, vol. 23, no. 3, pp. 717-726, Sep. 2008.

[11] F. Dubas and C. Espanet, "Analytical solution of the magnetic field in permanent-magnet motors taking into account slotting effect: no-load vector potential and flux density calculation," *IEEE Trans. Magn.*, vol. 45, no. 5, pp. 2097-2109, May. 2009.

[12] L. J. Wu, Z. Q. Zhu, D. Staton, M. Popescu, and D. Hawkins, "Subdomain model for predicting armature reaction field of surface-mounted permanent-magnet machines accounting for tooth-tips," *IEEE Trans. Magn.*, vol. 47, no. 4, pp. 812-822, Apr. 2011.

[13] X. Liu, H. Hu, J. Zhao, A. Belahcen, and L. Tang, "Armature reaction field and inductance calculation of ironless brushless dc motor," *IEEE Trans. Magn.*, vol. 52, no. 2, pp. 1-14, Feb. 2016.

[14] K. Shin, H. Cho, S. Lee, and J. Choi, "Armature reaction field and inductance calculations for a permanent magnet linear synchronous machine based on subdomain model," *IEEE Trans. Magn.*, vol. 53, no. 6, pp. 1-4, June 2017.

[15] H. Li, H. Hao, M. Jin, and J. Shen, "Analytical calculation of magnetic field distribution in magnetic gears with consequent-pole rotors by subdomain method," in *IEEE Vehicle Power and Propulsion Conf.*, Hangzhou, 2016.

[16] Y. Oner, Z. Q. Zhu, L. J. Wu, X. Ge, H. Zhan, and J. T. Chen, "Analytical on-load subdomain field model of permanent-magnet vernier machines," *IEEE Trans. Ind. Electron.*, vol. 63, no. 7, pp. 4105-4117, Jul. 2016.

[17] S. Teymoori, A. Rahideh, H. Moayed-Jahromi, and M. Mardaneh, "2-D analytical magnetic field prediction for consequent-pole permanent magnet synchronous machines," *IEEE Trans. Magn.*, vol. 52, no. 6, pp. 1-14, Jun 2016.

[18] A. Dalal, S. Nekkalapu, and P. Kumar, "2-D analytical subdomain model for hybrid dual-rotor motor," *IEEE Trans. Magn.*, vol. 52, no. 6, pp. 1-9, Jun. 2016.
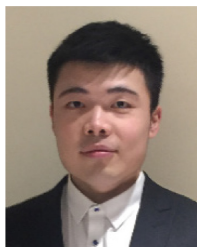
Minchen Zhu received the B.Eng degree in electrical engineering from Zhejiang University, Hangzhou, China, in 2015, where he has been working toward the Ph.D degree since 2015.

His current major research interests include the design and analysis of permanent magnet machines.

L.J. Wu (M'11-SM'14) received the B.Eng. and M.Sc. degrees from Hefei University of Technology, Hefei, China, in 2001 and 2004, respectively, and the Ph.D degree from the University of Sheffield, Sheffield, U.K., in 2011, all in electrical engineering. From 2004 to 2007, he was an Engineer with Delta Electronics (Shanghai) Co, Ltd. From 2012 to 2013, he was with Sheffield Siemens Wind Power Research Center as a design engineer focusing on wind power generators. From 2013 to 2016, he was an advanced engineer with Siemens Wind Power A/S in Denmark. Since 2016, he has been with Zhejiang University, where he is currently Professor of electrical machines and control systems. His current major research interests include design and control of permanent magnet machines.

Youtong Fang (M'11-SM'15) received the B.S. degree and Ph.D. degree in electrical engineering from Hebei University of Technology, Hebei, China, in 1984 and 2001 respectively.

Currently, he is a Professor with the College of Electrical Engineering, Zhejiang University, China. His research interests include the application, control, and design of electrical machines.

Thierry Lubin received the M.S. degree in electrical engineering from the University Pierre et Marie Curie, Paris, France, in 1994, and the Ph.D. degree from the University of Lorraine, Nancy, France, in 2003.

He is currently an Associate Professor of Electrical Engineering with the "Groupe de Recherche en Energie Electrique de Nancy", GREEN, Nancy, France.

His research interests include analytical modeling of electrical machines, contactless torque transmissions by magnetic gears and couplers, and the use of superconductors in electromechanical devices.